

MEASUREMENTS OF STELLAR INCLINATIONS FOR KEPLER PLANET CANDIDATES

TERUYUKI HIRANO¹, ROBERTO SANCHIS-OJEDA², YOICHI TAKEDA³, NORIO NARITA³, JOSHUA N. WINN², ATSUSHI TARUYA^{1,4,5}, AND YASUSHI SUTO^{1,4,6}

ABSTRACT

We present an investigation of spin-orbit angles for planetary system candidates reported by Kepler. By combining the rotational period P_s inferred from the flux variation due to starspots and the projected rotational velocity $V \sin I_s$ and stellar radius obtained by a high resolution spectroscopy, we attempt to estimate the inclination I_s of the stellar spin axis with respect to the line-of-sight. For transiting planetary systems, in which planetary orbits are edge-on seen from us, the stellar inclination I_s can be a useful indicator of a spin-orbit alignment/misalignment. We newly conducted spectroscopic observations with Subaru/HDS for 15 KOI systems, whose lightcurves show periodic flux variations. After detailed analyses of their lightcurves and spectra, it turned out that some of them are binaries, or the flux variations are too coherent to be caused by starspots, probably representing ellipsoidal variations, and consequently we could constrain stellar inclinations I_s for eight systems. Among them, KOI-262 and 280 are in good agreement with $I_s = 90^\circ$ suggesting a spin-orbit alignment, while at least one system, KOI-261, shows a possible spin-orbit misalignment. We also obtain a small I_s for KOI-1463, but the transiting companion seems to be a star rather than a planet. The results for KOI-257, 269, 367, and 974 are ambiguous, and can be explained with either misalignments or moderate differential rotation. Since our method can be applied to any system having starspots regardless of the planet size, future observations will allow for the expansion of the parameter space in which the spin-orbit relations are investigated.

Subject headings: planets and satellites: general – planets and satellites: formation – stars: rotation – techniques: spectroscopic

1. INTRODUCTION

The standard formation theory of close-in gas giants (hot-Jupiters) suggests that they form outside of the so-called “snow-line”, located at a few AU away from the host star, and subsequently migrate inward (e.g., Lin et al. 1996; Chambers 2009; Lubow & Ida 2010). While migration processes such as disk-planet interactions (type I or II migration) predict small orbital eccentricities of planets and small stellar obliquity (i.e. the angle between the stellar spin axis and the planetary orbital axis), dynamical processes including planet-planet scattering and/or Kozai cycles might produce large values for both eccentricity and stellar obliquity (e.g., Wu & Murray 2003; Fabrycky & Tremaine 2007; Nagasawa et al. 2008; Chatterjee et al. 2008; Nagasawa & Ida 2011).

Measurements of the Rossiter-McLaughlin effect (hereafter, the RM effect), which is an apparent radial velocity anomaly during a planetary transit, provide invaluable information to better understand the planetary migration process (Ohta et al. 2005; Winn et al. 2005;

Narita et al. 2007; Albrecht et al. 2007; Hébrard et al. 2008; Triaud et al. 2010; Hirano et al. 2011b). Through the RM effect, one can measure the sky-projected angle λ between the stellar spin axis and planetary orbital axis, which is of importance to distinguish among the possible migration channels.

So far, more than 40 transiting systems have been investigated to estimate λ , and many interesting correlations among spin-orbit angles and physical properties of planets and host stars have been proposed. Winn et al. (2010a) pointed out that a substantial spin-orbit misalignment tends to be observed around hot stars (whose effective temperatures $T_{\text{eff}} \gtrsim 6250$ K). This fact might be related to the tidal evolution of host star’s obliquities. Triaud (2011) also found a correlation between the stellar ages and obliquities, claiming that spin-orbit misalignments are observed around younger systems with ages less than 2.5 Gyr. This trend is consistent with what Winn et al. (2010a) found, suggesting that tidal interactions between the host stars and close-in giant planets, formed after some dynamical processes such as planet-planet scattering, gradually damp the obliquity of host stars close to 0° .

It should be noted that measurements of the RM effect are only feasible for rather bright stars ($V \lesssim 12$) with giant transiting planets. While detections of the RM effect for a super-Neptune were reported (Hirano et al. 2011a; Winn et al. 2010b), those for smaller planets ($R_p \lesssim 0.5R_J$) are still challenging. Nevertheless, in order to discuss planetary formation and migrations, it is of great interest to investigate the spin-orbit relations for systems with Neptune-sized or even Earth-sized exoplanets, which are reported to be more abundant than jovian planets (Borucki et al. 2011; Mayor et al. 2011).

Electronic address: hirano@utap.phys.s.u-tokyo.ac.jp

¹ Department of Physics, The University of Tokyo, Tokyo 113-0033, Japan

² Department of Physics, and Kavli Institute for Astrophysics and Space Research, Massachusetts Institute of Technology, Cambridge, MA 02139

³ National Astronomical Observatory of Japan, 2-21-1 Osawa, Mitaka, Tokyo, 181-8588, Japan

⁴ Research Center for the Early Universe, School of Science, The University of Tokyo, Tokyo 113-0033, Japan

⁵ Institute for the Physics and Mathematics of the Universe (IPMU), The University of Tokyo, Chiba 277-8582, Japan

⁶ Department of Astrophysical Sciences, Princeton University, Princeton, NJ 08544

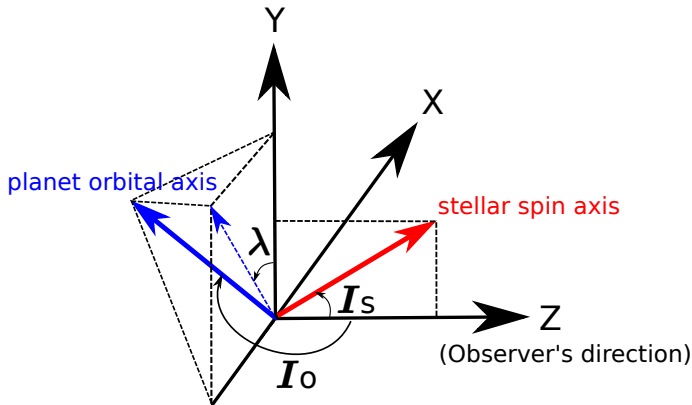


FIG. 1.— Schematic figure for the spin and orbital axes. In this figure, the $x-y$ plane indicates the sky plane and the z axis points toward us. The planet’s orbital axis is indicated by the blue arrow and its projection onto the sky plane is shown by the dashed arrow. The red arrow is the stellar spin axis, which is located in the $y-z$ plane.

In order to measure spin-orbit relations for such smaller planets, we focus on the Kepler photometry in this paper. The Kepler mission is an ambitious and very productive project designed to “determine the frequency of Earth-size planets in and near the habitable zone of solar-type stars”. As of March 2012, more than two thousand planetary candidates were announced by the Kepler team (Borucki et al. 2010, 2011; Batalha et al. 2012), and each of those stars having planetary candidate(s) is called Kepler Object of Interest (KOI). Among the published Kepler light curves, there are many systems that show periodic flux variations most likely due to starspots on the stellar surface (Basri et al. 2011). For those systems, a period analysis enables us to infer the rotational period P_s of the star. That rotational rate, along with the stellar radius R_s , can be directly translated into the rotational velocity at the equator of the star, V_{eq} in the absence of differential rotation. If we compare V_{eq} with the projected rotational velocity $V \sin I_s$ estimated by a spectroscopic observation, we can constrain the stellar inclination I_s , which is defined as the angle between the line-of-sight and the axis of the stellar rotation (see Figure 1). Since transiting planetary systems nearly have edge-on orbits seen from our location, the orbital inclination I_o (the angle between our line-of-sight and the planetary orbital axis) should be close to 90° . Therefore, a significant deviation of I_s from 90° implies a spin-orbit misalignment. This method to constrain the stellar obliquities will be described in detail in Section 2.

The statistics of the spin-orbit angles along the line-of-sight has been discussed by Schlaufman (2010). Using the empirical relation among the stellar ages, masses, and rotational periods, he statistically discussed the rotational velocity of the stars hosting transiting planets. He found that some of the transiting systems have smaller $V \sin I_s$ than expected for the case of spin-orbit alignment, and pointed out that it is most likely to be evidence of spin-orbit misalignments along the line-of-sight. In contrast to his analysis that relies on an empirical relation to estimate the rotational period P_s of the planet hosting stars, we attempt to derive it more directly for each of the KOI systems using the precise Kepler photometry. In order to constrain I_s , we newly conducted

high resolution spectroscopic observations and obtained spectra for 15 KOI systems using the Subaru telescope.

The remaining sections are organized as follows. In Section 2, we describe the basic method to estimate the spin-orbit angle along the line-of-sight in detail and discuss the pros and cons of the present method in comparison with the RM effect. We briefly describe the spectroscopic observations with Subaru in Section 3. Section 4 presents the photometric and spectroscopic analyses and their results. The correlations between the stellar inclinations and other system parameters are discussed in Section 5. Finally, Section 6 is devoted to summary and future prospects.

2. PRINCIPLE

If there exists a spot on the surface of a star, the lightcurve of the star exhibits a periodic variation due to the stellar rotation. A period analysis of the lightcurve enables us to estimate the rotational period P_s of the star. Figure 2 shows an example of the Kepler lightcurve (KOI-261) and its periodogram. The peak in the periodogram most likely reflects the rotational period P_s , which is estimated as $P_s = 15.4 \pm 0.3$ days. Once P_s is estimated, the stellar inclination I_s is estimated by the following relation:

$$I_s = \arcsin \left\{ \frac{P_s (V \sin I_s)_{\text{spec}}}{2\pi R_s} \right\}, \quad (1)$$

where $(V \sin I_s)_{\text{spec}}$ and R_s are the projected rotational velocity and the radius of the star, respectively. Both of these quantities are estimated via spectroscopy under the assumption that the star is rigidly rotating. The impact of differential rotation will be discussed in Section 5.

Since the configuration of the transiting system has an edge-on orbit seen from us (with the orbital inclination $I_o \gtrsim 85^\circ$), a small value of I_s implies a possible spin-orbit misalignment in the system, regardless of the sky-projected spin-orbit angle λ (see Figure 1). The 3D angle ψ between the stellar spin axis and planetary orbital axis is associated with I_s , I_o , and λ by the following equation (Fabrycky & Winn 2009):

$$\cos \psi = \sin I_s \cos \lambda \sin I_o + \cos I_s \cos I_o. \quad (2)$$

The present method has several advantages that we mention below. Although observations of the RM effect have enabled us to discover the spin-orbit misalignment for the first time and revealed its possible patterns in terms of stellar and planetary properties (Hébrard et al. 2008; Narita et al. 2009; Winn et al. 2009, 2010a; TriAUD 2011), the methodology is feasible only for sufficiently bright stars ($V \lesssim 12$) with giant transiting planets ($R_p \gtrsim 0.5 R_J$). In addition, a measurement of λ requires spectroscopic observations throughout a complete transit. Therefore the observation is time-critical and also time-consuming, in particular for those systems in which the semi-major axis of the planet is large and the transit duration is long.

In contrast, the current method of measuring spin-orbit relations uses the effect of stellar spots induced by rotation on the flux of the star, and thus requires only one spectroscopic observation independently of the size of planets and their semi-major axes. Therefore the present method is more efficient in increasing the number of samples, and should expand the parameter space in which spin-orbit relations are investigated.

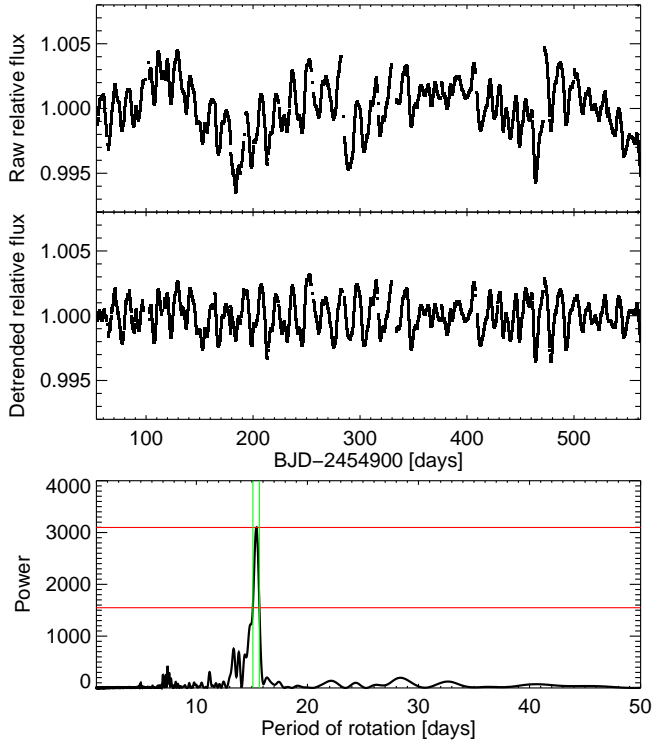


FIG. 2.— *Top.* - Quarter by quarter mean normalized raw out-of-transit flux of KOI-261 (PDCSAP_FLUX). Includes quarters 0 through 6, except quarter 5 where this target was not observed. *Central.* - Detrended flux of the star, obtained with the method described in Section 4. *Bottom.* - Lomb-Scargle periodogram of the detrended flux. The solid vertical lines represent the points where the power is half of the maximum power. The final value is taken to be the mean of these points, and the error to be half of their difference.

In systems where spots are present, there is a possibility that the planet passes in front of one of them during a transit. The recurrence of these spot-crossing events at consecutive transits proves that the system has a low spin-orbit angle (Sanchis-Ojeda et al. 2011; Nutzman et al. 2011; Désert et al. 2011). However, to locate the spot anomalies for this spot-crossing method requires a high signal-to-noise ratio for the transit lightcurve, which is achievable only for large planets or very bright stars. Also it would be more suitable for cool stars where active regions tend to be larger and produce more visible spot anomalies. In addition to this, cool stars generally have a lower $V \sin I_s$, which complicates the use of our method.

On the other hand, measuring the spin-orbit relation along the line-of-sight with the present technique has a few shortcomings. First, because of the shape of the sine function, the uncertainty for I_s tends to be larger when $\sin I_s$ is close to unity. Second, it is impossible to distinguish the state of I_s from that of $\pi - I_s$, which gives exactly the same value of $\sin I_s$. This is a marked contrast with the RM measurements, through which we can clearly distinguish between the prograde and retrograde orbits at least on the sky.

Finally, types of stars to which we can apply our present technique are fairly limited. According to the survey by Radick et al. (1982), the flux variations due to dark starspots are only seen in Sun-like stars whose

effective temperatures are up to 6400 K, with a photometric precision of ~ 3 mmag. Therefore, if we observe a periodic flux variation with a large amplitude for an early type star hotter than 6500 K, it is more likely to be spurious, possibly reflecting a flux contamination by a companion star or faint background sources. Therefore the present method is complementary to the RM effect, in the sense that RM measurements are applicable to even hotter stars (e.g., Collier Cameron et al. 2010).

There are some systems in which spots were used to estimate rotational periods of the planet-hosting stars (e.g., Lanza et al. 2009; Désert et al. 2011, for CoRoT-2 and Kepler-17, respectively). Specifically, Hébrard et al. (2011) applied the present technique to investigate the spin-orbit relations to the CoRoT-18 system, and obtained a weak constraint on the stellar inclination as $I_s = 70^\circ \pm 20^\circ$. This was in good agreement with the small value of the sky-projected spin-orbit angle ($\lambda = 10^\circ \pm 20^\circ$), implying a 3D spin-orbit alignment. In this paper, we systematically apply this technique to some of the KOI systems showing periodic flux variations.

3. OBSERVATION

We applied the following three criteria to all the KOI systems in the February 2011 data release (Borucki et al. 2011), and selected 15 KOI systems (KOI-4, 42, 100, 257, 258, 261, 262, 269, 279, 280, 302, 367, 974, 1020, 1463); 1) the lightcurve exhibits flux variations by a visual inspection, 2) the (photometrically estimated) effective temperature is higher than ~ 6000 K, and 3) the Kepler magnitude is brighter than $K_p \sim 13.0$. The second criterion is adopted since hotter stars are likely to have larger $V \sin I_s$ and so the relative statistic and systematic errors in I_s become smaller.

In order to derive spectroscopic parameters for those KOI systems, we conducted spectroscopic observations with the High Dispersion Spectrograph (HDS) installed on the Subaru telescope, located in Hawai'i. The observations were performed on June 12, July 23, 24, and October 19, 2011 (UT). We employed the I2a observing mode, which covers the wavelength regions of 4950 Å to 6150 Å (blue CCD) and 6400 Å to 7550 Å (red CCD). The spectral resolutions were set as $R \sim 90,000$ on June 12 and July 24, $R \sim 60,000$ on July 23, and $R \sim 110,000$ on October 19, respectively. The resolution for each target is summarized in the middle column of Table 1. The seeing on each observing nights was typically 0.5 – 0.8 arcseconds.

On each of those observing nights, we obtained the reference spectrum of the flat lamp transmitted through the Iodine cell, using the same setup (spectral resolution). These reference spectra were used to reproduce the instrumental profile for each spectral resolution, and then play a crucial role in estimating the projected rotational velocity $V \sin I_s$ for slowly rotating stars.

We reduced the raw data of each spectrum using the standard IRAF procedure. The resulting spectra have the typical signal-to-noise ratio (SNR) of 80 – 120 per pixel after extracting the 1D spectra.

4. ANALYSES AND RESULTS

4.1. Estimation of Rotational Periods

In order to determine the periods of photometric variations, we used all public data available from the MAST archive for the 15 targets. In most cases, quarters 0 through 6 were available, corresponding to 500 days of observations in total. In this analysis, only the long cadence observations were used, which proved to be sufficient to study the flux variability with a timescale of a few days. Since the PDC pipeline is known to remove partially or totally the stellar flux variability on the timescales we are interested in (Jenkins et al. 2010b), we decided to use the raw flux, named SAP_FLUX in the version 2.0 of the FITS files delivered by the Kepler team. Note that the newest improvements on the Kepler pipeline (Stumpe et al. 2012; Smith et al. 2012) also seem to allow for a fast identification of the real astrophysical noise, but we simply apply the method below in the present paper.

We used the linear ephemeris of all planet candidates published in the February 2011 data release (Borucki et al. 2011) to locate all transits and remove them from the flux series. Then, using a smoothed version of the flux where each point is the average of the previous and next 10 points, we estimate the standard deviation of the flux, and we applied 3 sigma clipping to the data in order to remove outliers. Raw Kepler data suffer from several well known instrumental artifacts (Jenkins et al. 2010c) that would not be corrected by the 3 sigma clipping. Some of them only affect a certain interval of the observations, for example the changes in flux due to temperature drifts after the telescope points to the Earth.

There are also long term trends due to the constant movement of the targets on the CCD. In order to remove them, we detrend the data using the cotrending basis vectors, following the instructions from the Data Release 12 Notes. These cotrending vectors are constructed to capture most of the flux variability caused by instrumental artifacts in each CCD. The mean-subtracted, mean-normalized flux of each target can be considered as a superposition of the astrophysical flux of the star plus a linear combination of these orthonormal basis of cotrending vectors. Assuming that the astrophysical flux is orthogonal to the instrumental noise, we can estimate the coefficients of the linear combination by simply taking the vector product of the mean-subtracted, mean-normalized raw flux with as many cotrending vectors as needed to clean the lightcurve. After this removal, we added back the previously subtracted mean, to then normalize by the mean each quarter to avoid differences in flux from quarter to quarter.

We applied the above procedure to the 15 targets, and studied the final flux lightcurve. Visual inspection of the light curves confirmed the existence of flux variability due to starspots on 13 out of the 15 cases, with periodic signals with amplitudes and phases that evolve with time. KOI-258 and KOI-302 show a very clear but coherent variability that does not change shape with time. Such strictly periodic signals are unlikely to be caused by spots, especially in the case of KOI-258 where the period of the signal is equal to the orbital period of the candidate. This strongly suggests that the periodic dimming of KOI-258 is likely to be caused by a background binary.

In order to estimate the periods of rotation for the rest of the stars, we use a lomb-scargle algorithm and

TABLE 1
SPECTRAL RESOLUTIONS ADOPTED IN SPECTROSCOPIC
OBSERVATIONS BY SUBARU/HDS AND ROTATIONAL PERIODS
ESTIMATED BY THE KEPLER PHOTOMETRY.

System	R	P_s (days)
KOI-4	~ 110000	5.65 ± 0.03
KOI-42	~ 90000	20.84 ± 0.37
KOI-100	~ 90000	1.132 ± 0.002
KOI-257	~ 90000	7.846 ± 0.052
KOI-258	~ 90000	too coherent
KOI-261	~ 110000	15.38 ± 0.30
KOI-262	~ 90000	8.171 ± 1.218
KOI-269	~ 90000	5.351 ± 0.136
KOI-279	~ 90000	20.92 ± 0.93
KOI-280	~ 90000	15.78 ± 2.12
KOI-302	~ 60000	too coherent
KOI-367	~ 90000	27.65 ± 3.56
KOI-974	~ 110000	10.83 ± 0.12
KOI-1020	~ 90000	10.91 ± 1.06
KOI-1463	~ 60000	6.042 ± 0.042

analyze the power spectra of the stellar fluxes. A high peak is expected to happen at the period of rotation of the star, although a strong peak can also appear at half the period if several spots are present. The peak can also be rather wide if differential rotation is present, or even be composed of several peaks. However, visual inspection can also reveal important information about the periodic behavior of the flux series, and it helped to identify a few cases where indeed the highest peak corresponded to half the period of rotation. In these cases, two similar spots, with opposite stellar longitudes, induce flux variations with twice the frequency. The evolution of the size of both spots, which creates asymmetries between the flux variations induced by both, allows us to identify them unambiguously.

The final values of the period of rotation and their errors are obtained by studying the proximity of the strongest peak, and summarized in the right column of Table 1. We adopt the full-width at half maximum (FWHM) of the peak as the 1-sigma error, with the center of the interval being the rotation period. Note that if a differential rotation produces several peaks with similar amplitudes at similar periods, the resulting merged peak in the periodogram is broadened, and the above assigned error becomes large. Thus, the presence of stellar differential rotation makes the estimate of the period less accurate.

4.2. Estimation of Spectroscopic Parameters

Following Takeda et al. (2002, 2005), we analyze each spectrum and estimate the effective temperature T_{eff} , surface gravity $\log g$, microturbulence ξ , and metallicity $[\text{Fe}/\text{H}]$ by measuring the equivalent widths of Fe I and Fe II lines. In order to accurately estimate $V \sin I_s$ with avoiding any systematic effect, we numerically integrate each component on the stellar disk Doppler-shifted due to stellar rotation and macroturbulence. In doing so, we also convolve the intrinsic (thermal motion + microturbulence) profile with the rotational and macroturbulence broadening function and the instrumental profile to reproduce the observed spectrum.

For macroturbulence, we adopt the radial-tangential

model (Gray 2005). For the given macroturbulence dispersion ζ_{RT} and the stellar limb-darkening parameter ($\epsilon = 0.6$), we determine the best-fit solution of $V \sin I_s$ for each of the spectra. Since the macroturbulence dispersion ζ_{RT} is not well understood, especially for hotter stars, we try several different values of ζ_{RT} . For the final result, we adopt the following empirical expression by Valenti & Fischer (2005):

$$\zeta_{\text{RT}} = \left(3.98 + \frac{T_{\text{eff}} - 5770 \text{ K}}{650 \text{ K}} \right) \text{ km s}^{-1}, \quad (3)$$

and estimate the systematic uncertainty for $V \sin I_s$ by changing ζ_{RT} by $\pm 15\%$ from Equation (3) for cool stars ($T_{\text{eff}} \leq 6100 \text{ K}$) based on the observed distribution of ζ_{RT} (see Figure 3 in Valenti & Fischer 2005). For the case of hotter stars ($T_{\text{eff}} > 6100 \text{ K}$), however, the macroturbulence is not intensely investigated and thus we conservatively estimate the systematic error for $V \sin I_s$ by changing ζ_{RT} by $\pm 25\%$. The statistical errors in fitting each spectrum are generally smaller than the systematic errors arising from different values of ζ_{RT} .

As for the instrumental profile, we basically adopt Gaussian broadening functions whose FWHMs correspond to each of the spectral resolutions adopted in the observations ($R \sim 60,000, 90,000, \text{ and } 110,000$). In the case of slowly rotating stars ($V \sin I_s \lesssim 5 \text{ km s}^{-1}$), however, we found that the shape of the instrumental profile, which is slightly different from Gaussian, sometimes affects the estimate of $V \sin I_s$. Thus, we convolve the actual shapes of the instrumental profile estimated by the reference transmission spectrum of the Iodine cell for those slow rotators (i.e., KOI-261 and KOI-367).

Takeda (1995) applied this procedure to the high-resolution solar flux spectrum and obtained the solar spin velocity of $V \sin I_s = 2.00 \pm 0.34 \text{ km s}^{-1}$. Since the angular velocity around the solar equator is about $14^\circ \text{ day}^{-1}$ from the observations of spatially resolved spots (Ruždjak et al. 2005), we obtain $V_{\text{eq}} \approx 2.0 \text{ km s}^{-1}$ for the Sun. We also applied this technique to the spectrum of HAT-P-11, whose rotational velocity is reported to be very small ($V \sin I_s = 1.00^{+0.95}_{-0.56} \text{ km s}^{-1}$, Winn et al. 2010b) from the measurement of the RM effect, independent of the spectral line analysis. Although the resolution of HAT-P-11's spectrum that we analyzed is relatively low ($R \sim 45000$), we obtained $V \sin I_s = 1.79 \pm 0.65 \text{ km s}^{-1}$ from the line analysis (including the convolution of the instrumental profile), which is consistent with the result estimated by the RM measurement. These two tests (for the Sun and HAT-P-11) validate the present technique to estimate $V \sin I_s$ for slow rotators. Of course, they do not guarantee the extrapolation of even smaller $V \sin I_s$ ($\lesssim 1.0 \text{ km s}^{-1}$, e.g., KOI-261), but for such stars, we can safely rule out a large $V \sin I_s$ ($\gtrsim 2 \text{ km s}^{-1}$) with a high confidence level.

Once T_{eff} , $\log g$, and $[\text{Fe}/\text{H}]$ are given, we can estimate the stellar age, mass M_s , and radius R_s for each system. We here employ the Yonsei-Yale (Y^2) isochrone model to estimate these parameters (Yi et al. 2001). The result is summarized in Table 2. A visual inspection of the spectrum indicates that KOI-1020 is a spectroscopic binary, which makes it difficult to derive spectroscopic parameters. In addition, the rotational velocities of KOI-4, 100, 258, and 366, are so large ($V \sin I_s > 30 \text{ km s}^{-1}$) that

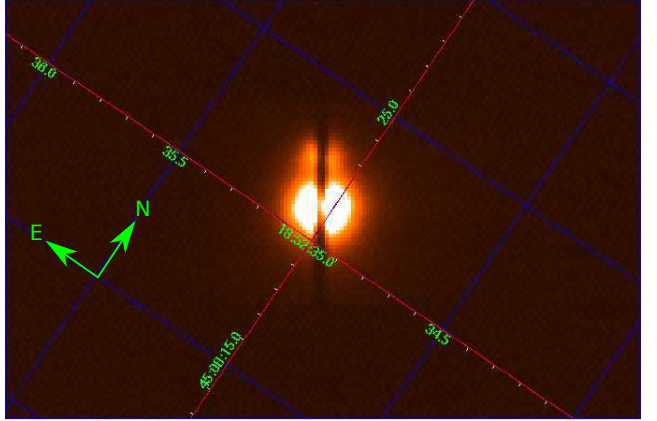


FIG. 3.— The slit viewer image for KOI-42. A companion star is seen about $2.0''$ to the north-east of the main star. The companion star is on the slit.

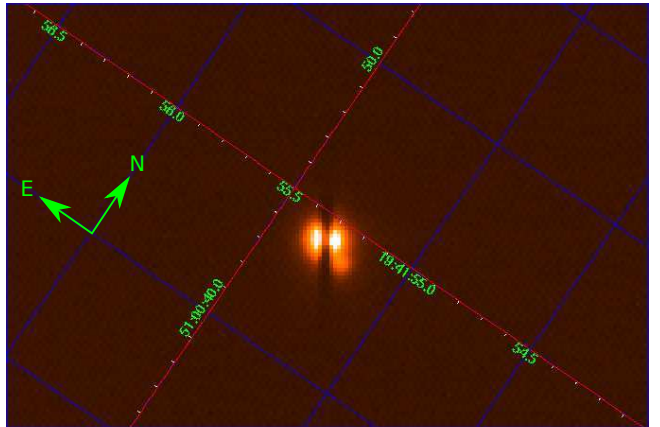


FIG. 4.— The slit viewer image for KOI-279. A companion star is seen about $1.5''$ to the west of the main star. The light from the companion is partly on the slit.

their spectra look very flat, which prohibits any reliable estimates of the atmospheric parameters (T_{eff} , $\log g$, ξ , and $[\text{Fe}/\text{H}]$) with our current SNR's. The best-fit values of $V \sin I_s$ for those systems are estimated as 39.0 km s^{-1} , 32.8 km s^{-1} , 134.5 km s^{-1} , and 34.1 km s^{-1} , for KOI-4, 100, 258, and 366, respectively. For such rapid rotators, asymmetries in the transit lightcurve may be used to determine the parameters only if the spin-orbit angle is large (Barnes 2009). Such an analysis is beyond the scope of this paper, and we do not perform it here.

Regarding KOI-42 and KOI-279, the estimated values of $\log g$ seem too large for stars with T_{eff} of $\sim 6500 \text{ K}$ (e.g., see Figure 2 in Fuhrmann 1998). These large values of $\log g$ may explain the unusually young estimates for system ages listed in Table 2. This tends to be caused by blending of light by a companion star or another background source. Thus, we checked the slit viewer images for those targets taken simultaneously with the spectra, and consequently we found stellar companions for both of the systems and those companions seem to be on the slit of Subaru/HDS, causing significant contaminations in the spectra of KOI-42 and KOI-279 (see Figure 3 and 4). Kepler's photometric aperture is relatively large, which means that these companion stars are a big source of contamination. This increases the chance that the ro-

TABLE 2
SPECTROSCOPIC PARAMETERS. STARRED SYSTEMS HAVE COMPANION STARS, MOST LIKELY CAUSING CONTAMINATIONS IN SPECTRA.

System	T_{eff} (K)	$\log g$	[Fe/H]	age (Gyr)	M_s (M_{\odot})	R_s (R_{\odot})	$V \sin I_s$ (km s $^{-1}$)	V_{eq} (km s $^{-1}$)
KOI-42*	6512 \pm 58	4.542 \pm 0.090	0.114 \pm 0.050	< 0.06	1.373 \pm 0.022	1.293 $^{+0.045}_{-0.044}$	13.40 \pm 0.22	3.14 \pm 0.12
KOI-257	6218 \pm 28	4.286 \pm 0.055	0.154 \pm 0.031	2.00 $^{+0.38}_{-0.65}$	1.285 $^{+0.031}_{-0.021}$	1.347 $^{+0.105}_{-0.093}$	7.09 \pm 0.49	8.69 $^{+0.68}_{-0.60}$
KOI-261	5708 \pm 13	4.329 \pm 0.030	0.048 \pm 0.019	6.52 $^{+0.42}_{-0.35}$	1.057 $^{+0.009}_{-0.010}$	1.165 $^{+0.045}_{-0.046}$	0.62 $^{+1.09}_{-0.62}$	3.83 $^{+0.16}_{-0.17}$
KOI-262	6150 \pm 53	3.994 \pm 0.100	-0.104 \pm 0.047	3.27 $^{+0.60}_{-0.52}$	1.374 $^{+0.091}_{-0.083}$	1.963 $^{+0.280}_{-0.257}$	10.58 \pm 0.22	12.16 $^{+2.86}_{-2.19}$
KOI-269	6371 \pm 50	4.160 \pm 0.090	0.011 \pm 0.049	2.21 $^{+0.21}_{-0.30}$	1.382 $^{+0.080}_{-0.062}$	1.616 $^{+0.227}_{-0.193}$	11.62 \pm 0.22	15.28 $^{+2.19}_{-1.85}$
KOI-279*	6531 \pm 58	4.425 \pm 0.100	0.313 \pm 0.063	< 0.17	1.450 $^{+0.028}_{-0.022}$	1.258 $^{+0.110}_{-0.110}$	12.14 \pm 0.27	3.08 $^{+0.17}_{-0.17}$
KOI-280	6047 \pm 40	4.262 \pm 0.080	-0.258 \pm 0.034	5.16 $^{+0.69}_{-0.90}$	1.095 $^{+0.034}_{-0.024}$	1.279 $^{+0.141}_{-0.123}$	3.52 \pm 0.50	4.12 $^{+0.79}_{-0.62}$
KOI-302	6616 \pm 63	3.882 \pm 0.100	0.097 \pm 0.054	1.33 $^{+0.15}_{-0.13}$	1.773 $^{+0.110}_{-0.117}$	2.524 $^{+0.398}_{-0.350}$	16.66 \pm 0.16	N/A
KOI-367	5667 \pm 20	4.279 \pm 0.040	0.151 \pm 0.031	6.95 $^{+0.77}_{-0.79}$	1.071 $^{+0.016}_{-0.013}$	1.243 $^{+0.055}_{-0.059}$	1.04 \pm 0.74	2.27 $^{+0.36}_{-0.28}$
KOI-974	6385 \pm 30	4.058 \pm 0.050	-0.026 \pm 0.031	2.27 $^{+0.12}_{-0.14}$	1.464 $^{+0.051}_{-0.047}$	1.871 $^{+0.145}_{-0.133}$	7.13 \pm 0.49	8.74 $^{+0.69}_{-0.63}$
KOI-1463	6578 \pm 70	3.886 \pm 0.105	0.018 \pm 0.069	1.48 $^{+0.12}_{-0.17}$	1.725 $^{+0.122}_{-0.116}$	2.479 $^{+0.416}_{-0.359}$	9.66 \pm 0.36	20.76 $^{+3.49}_{-3.00}$

tational periods estimated by spots are biased and might reflect the companions' rotational periods. Therefore, we simply ignore these two systems in the following analysis and discuss the stellar inclinations for the rest of the systems.

We also checked the slit viewer images for the other targets to see if any contamination sources are located around the main objects. Consequently, we found that KOI-258 seems to have a companion star, located $\sim 1''$ to the east of the main object. This is consistent with our expectation from the photometric analysis in Section 4.1. In addition, the point spread function (PSF) of KOI-1020 looked distorted, which suggests existence of a companion or background sources. We could not locate any companion (within $\sim 1''$) nor anomalous PSF for the other systems.

We compare our result for the stellar parameters in Table 2 with the public KIC parameters, which are based on the photometric analyses. We find that the root-mean-square (RMS) differences between our result and KIC values for T_{eff} and $\log g$ are 217 K and 0.231 dex, respectively. These values are reasonably in good agreement with the reported uncertainties for the KIC parameters (~ 200 K and ~ 0.4 dex, respectively, Brown et al. 2011). Moreover, when we remove the possibly contaminated systems (KOI-42, 279, and 1463), the RMS differences significantly improve and become 101 K and 0.134 dex for T_{eff} and $\log g$, respectively.

4.3. Evidence of Possible Spin-Orbit Misalignments

After excluding the systems for which we could not estimate either the rotational period or the stellar radius, we are left with KOI-42, 257, 261, 262, 269, 279, 280, 367, 974, 1463. KOI-42 and KOI-279 were excluded as well because of the contaminations by companion stars, as mentioned above. In the right column of Table 2, we also show the rotational velocity at the stellar equator V_{eq} based on P_s obtained by the Kepler photometry and spectroscopically measured R_s . In Figure 5, we plot the projected rotational velocity $V \sin I_s$ as a function of V_{eq} . In this plot, we also show the three lines indicating $I_s = 90^\circ$, $I_s = 45^\circ$, and $I_s = 30^\circ$. While KOI-262 and KOI-280 are consistent with $I_s = 90^\circ$, the other systems are inconsistent with $I_s = 90^\circ$ within 1σ . In particular, KOI-261 and KOI-1463 have significantly small stellar inclinations. We note that KOI-262 is a multiple transiting system (candidate), which makes the system a very important sample to discuss planetary migrations.

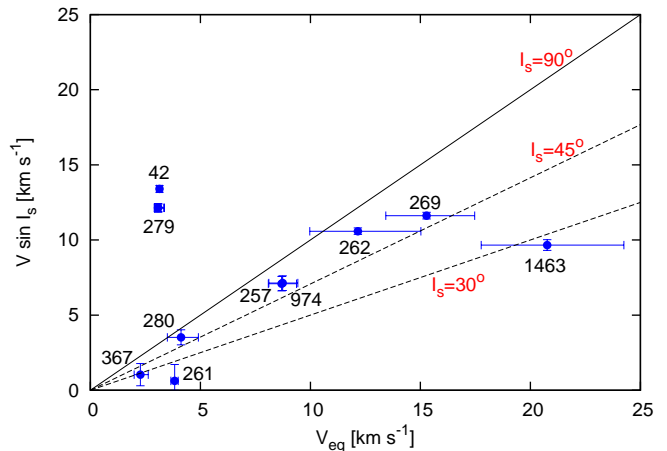


FIG. 5.— The estimated V_{eq} and $V \sin I_s$. The solid line indicates the case that our line-of-sight is vertical to the stellar spin axis. We also plot the two inclined cases in which $I_s = 45^\circ$ and 30° .

As for the KOI-1463 system, for which we inferred a small $\sin I_s$, the effective temperature of the host star ($\gtrsim 6500$ K) seems too high to have dark starspots, as mentioned in Section 2. This means that the periodic flux variation of KOI-1463 may be spurious, implying that the flux variations do not originate from the main star (with $T_{\text{eff}} > 6500$ K), although it is still possible that smaller spots (or spots with a higher brightness) induced the flux variation. Indeed the planet-to-star size ratio of KOI-1463 is reported to be $R_p/R_s = 0.13655$ from the Kepler transit lightcurve, and the radius of the transiting companion becomes $36.93^{+5.34}_{-6.21} R_{\oplus}$ when we simply substitute the stellar radius estimated via spectroscopy. An object with such a huge radius corresponds to a very late-type star rather than a planet. If this is the case, the periodic flux variation may come from the late-type companion star, KOI-1463.01, which may well be active enough to have starspots. Although the huge discrepancy between the public KIC parameter, which reports $R_s = 1.17 R_{\odot}$, and our estimate further supports this scenario, further lightcurve analyses and/or a high resolution imaging are required in order to understand the origin of the flux variation of KOI-1463.

While I_s is just an angle between the stellar spin axis and the line-of-sight, a small value of I_s (or $\sin I_s$) for transiting systems implies a spin-orbit misalignment, but not vice versa. To see this more clearly, let us consider

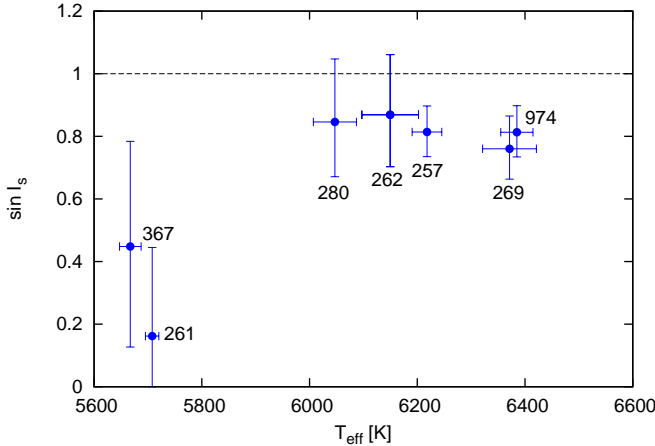


FIG. 6.— Correlation between the stellar inclination and stellar effective temperature.

the 3D spin-orbit angle ψ using Equation (2) again. Recall first that the orbital inclination I_o is expressed as

$$\cos I_o = b \frac{R_s}{a_p} \left(\frac{1 + e \sin \varpi}{1 - e^2} \right), \quad (4)$$

where b , a_p , e , ϖ are the transit impact parameter, planet’s semi-major axis, orbital eccentricity, and longitude of the periastron. Except for extremely eccentric planets ($e \gtrsim 0.9$), we expect that the right-hand-side of Equation (4), apart from the factor b , is of the order of R_s/a_p and b varies from zero to unity by definition. Therefore,

$$\cos I_o \lesssim \frac{R_s}{a_p}. \quad (5)$$

Substituting the above relation into Equation (2), we obtain

$$\begin{aligned} \cos \psi &= \sin I_s \cos \lambda \sin I_o + \cos I_s \cos I_o \\ &\lesssim \sin I_s + \frac{R_s}{a_p} \cos I_s. \end{aligned} \quad (6)$$

Equation (6) gives a lower limit of ψ from the observed value of I_s . For instance, in the case of KOI-261, we obtain $\psi \gtrsim 61^\circ$ based on Equation (6).

On the other hand, $I_s = 90^\circ$ (i.e., $\sin I_s = 1$) within its uncertainty does not necessarily mean a spin-orbit alignment. This is analogous to the case of $\lambda = 0^\circ$ for an RM measurement, which does not always imply a spin-orbit alignment. Statistical treatments are important in both cases in order to compare observed distributions with planetary migration theories.

5. DISCUSSION

5.1. Correlation between Stellar Inclinations and Other System Parameters

In the previous section, we have shown that at least one system (KOI-261) out of our 15 targets indeed indicates a possible spin-orbit misalignment along the line-of-sight. KOI-1463 also indicates a small inclination, but given the facts that its companion is more likely a star rather than a planet and its effective temperature is too high for KOI-1463 to have starspots, the inferred rotational velocity

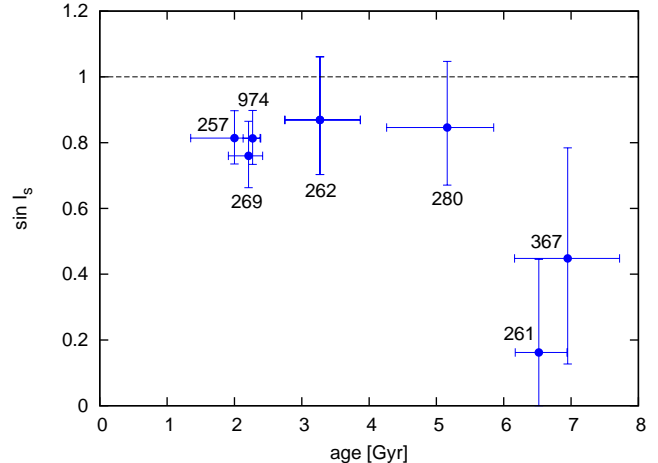


FIG. 7.— Correlations between the stellar inclination and stellar age.

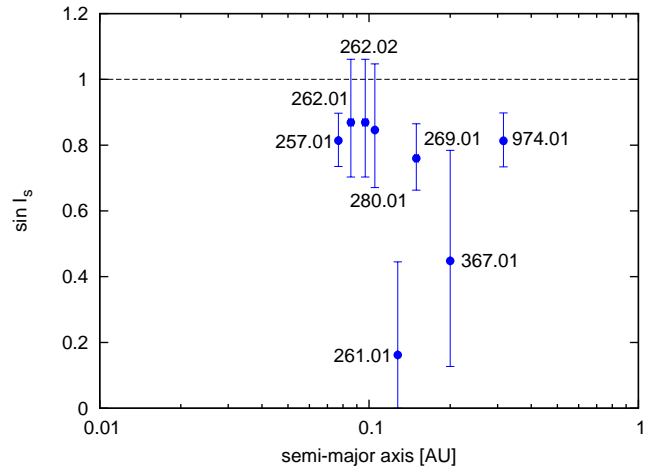


FIG. 8.— Correlation between the stellar inclination and semi-major axes of planets.

at the stellar equator V_{eq} is suspicious. Therefore, we do not further consider the KOI-1463 system with currently available data. Other systems (KOI-257, 269, 974) also show possible spin-orbit misalignments with $\gtrsim 2\sigma$, but those moderate spin-orbit misalignments may be caused by stellar differential rotations as we will show later in Section 5.3. Before discussing the impact of differential rotation, we here discuss the dependences of I_s (that tells us about spin-orbit relations) on the system parameters.

Figure 6 and 7 plot the stellar inclinations $\sin I_s$ against the stellar effective temperatures T_{eff} and their ages, respectively. As mentioned in Section 1, host stars’ effective temperatures and ages are reported to have significant correlations with stellar obliquities (Winn et al. 2010a; Triaud 2011). Amongst all, KOI-261 does not seem to follow the possible patterns by Winn et al. (2010a) and Triaud (2011), who suggested that spin-orbit misalignments are seen around hot, young stars, although KOI-261 has only a Neptune-sized planetary candidate as shown later in this subsection.

Next, in order to get a clearer insight into each of the systems, we would like to provide a rough estimate for

TABLE 3
CORRELATION BETWEEN $\sin I_s$ AND PLANETARY PARAMETERS.

Planetary Candidate	$\sin I_s$	P_o (days) (adopted)	R_p/R_s (adopted)	a_p (AU)	$R_p (R_{\oplus})$
KOI-257.01	$0.814^{+0.083}_{-0.079}$	6.883403 ± 0.000012	0.02052 ± 0.00015	$0.0769^{+0.0007}_{-0.0004}$	$3.01^{+0.24}_{-0.21}$
KOI-261.01	$0.162^{+0.283}_{-0.162}$	16.238480 ± 0.000019	0.02431 ± 0.00033	0.1278 ± 0.0004	$3.09^{+0.13}_{-0.33}$
KOI-262.01	$0.869^{+0.192}_{-0.166}$	7.8125124 ± 0.000052	0.01074 ± 0.00015	$0.0856^{+0.0019}_{-0.0017}$	$2.29^{+0.30}_{-0.42}$
KOI-262.02	$0.869^{+0.192}_{-0.166}$	9.376137 ± 0.000056	0.01362 ± 0.00030	$0.0967^{+0.0021}_{-0.0020}$	$2.91^{+0.38}_{-0.27}$
KOI-269.01	$0.760^{+0.105}_{-0.097}$	18.01134 ± 0.00022	0.01074 ± 0.00019	$0.1497^{+0.0029}_{-0.0022}$	$1.89^{+0.23}_{-0.32}$
KOI-280.01	$0.846^{+0.201}_{-0.175}$	11.872914 ± 0.000023	0.01972 ± 0.00073	$0.1050^{+0.0010}_{-0.0008}$	$2.75^{+0.28}_{-0.59}$
KOI-367.01	$0.448^{+0.336}_{-0.321}$	31.578680 ± 0.000018	0.0420 ± 0.0038	$0.2000^{+0.0010}_{-0.0008}$	$5.69^{+0.57}_{-0.21}$
KOI-974.01	$0.813^{+0.085}_{-0.079}$	53.50607 ± 0.00061	0.01353 ± 0.00014	$0.3155^{+0.0037}_{-0.0034}$	$2.76^{+0.20}_{-0.21}$
KOI-1463.01	$0.465^{+0.080}_{-0.069}$	N/A	0.13655	N/A	$36.93^{+6.21}_{-5.34}$

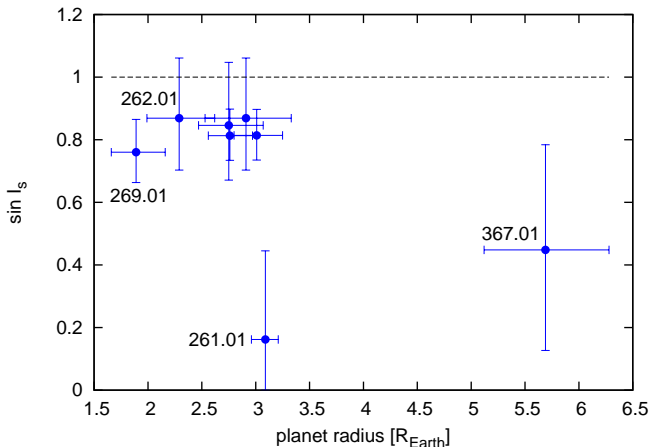


FIG. 9.— Correlation between the stellar inclination and planetary radii.

planetary parameters by using the public photometric data. First, we focus on the semi-major axes of the planets. The distance between the planet and its host star plays a critical role in discussing planetary migrations, tidal interactions, and the resultant stellar obliquities with respect to planetary orbits. As usual, the planet semi-major axis a_p is written as

$$a_p = \left(\frac{P_o}{2\pi} \right)^{2/3} \frac{(GM_s)^{1/3}}{\left(1 + \frac{M_p}{M_s} \right)^{2/3}}, \quad (7)$$

where G is the gravitational constant, and P_o and M_p are the orbital period and planet mass, respectively. Now that we have a better estimate for the stellar mass M_s from spectroscopy, we substitute M_s in Table 2 into the above equation. Adopting the public orbital period for each of the KOI planetary candidates from the MAST archive (as of March 2012), and neglecting the term of M_p/M_s ($\lesssim 0.001$), we obtain the semi-major axis a_p shown in Table 3. We plot the stellar inclination $\sin I_s$ for each planetary candidate as a function of the semi-major axis a_p in Figure 8.

Finally, we deal with the planet radius. From the transit lightcurve, it is generally possible to estimate the size of the transiting planet relative to the stellar radius, but since the systems on which we are focusing are only candidates, we need to keep in mind that lightcurve may be

blended with the flux from a binary companion or other background sources. In particular, because of the relatively large aperture size of the Kepler photometry, some of the systems may well be blended. We visually checked each of the spectra obtained by Subaru/HDS and found that none of the remaining systems (i.e., KOI-257, 261, 262, 269, 280, 367, and 974) seems to be a spectroscopic binary (SB2), though blending scenarios by faint companions or background sources are still possible. Further observations are required in order to rule out the binary scenario. Here, we simply adopt the planet-to-star size ratios R_p/R_s reported by the Kepler team, and infer the planet radii using the spectroscopically estimated stellar radii.

The result is also shown in Table 3 and its correlation with $\sin I_s$ is plotted in Figure 9. Most of the candidates seem to be super-Earths or Neptune-sized planets. As for the two Neptune-sized planets orbiting relatively cool stars, the orbit of KOI-261.01 seems to be inclined with respect to the spin axis of the host star, as in the case of the super-Neptune HAT-P-11b, for which a significant spin-orbit misalignment around a cool star was found through the RM measurements (Winn et al. 2010b; Hirano et al. 2011a) and a precise photometric analysis of the effect of spots in the transit light curves (Sanchis-Ojeda & Winn 2011). As we have noted in Section 1, giant planets (including Neptune-sized ones) discovered inside of the snow line (\sim a few AU) should have experienced planetary migrations. The possible spin-orbit misalignments in the KOI-261 system suggests that in some of the systems with close-in Neptune-sized planets, planet-planet scatterings or other dynamical processes such as the Kozai cycles may have played important roles during their formations and evolutions.

5.2. Comparison with Empirical Estimates for P_s

We have estimated the stellar rotational period P_s based on the periodic analysis of the Kepler photometry. While the current method is valid as long as the periodic flux variation comes from the spot on the stellar surface, the variation may be due to some other sources such as flux variations of background stars. In order to check the reliability of P_s that we estimated, we apply the gyrochronological method as employed by Schlaufman (2010). We simply adopt the same empirical relation for the rotational period as a function of the stellar mass M_s and age. Substituting M_s and ages listed in Table 2 into the empirical formula by Schlaufman (2010), we obtain

TABLE 4

ROTATIONAL PERIODS ESTIMATED BY THE EMPIRICAL RELATION.

System	P_s (days)	$P_{s,model}$ (days)	Flux Variability (%)
KOI-257	7.846 ± 0.052	$6.56^{+0.59}_{-0.79}$	0.1511
KOI-261	15.38 ± 0.30	$25.98^{+0.75}_{-0.74}$	0.3357
KOI-262	8.171 ± 1.218	$6.51^{+2.80}_{-1.82}$	0.0520
KOI-269	5.351 ± 0.136	$5.06^{+0.95}_{-0.91}$	0.0213
KOI-280	15.78 ± 2.12	$20.33^{+2.61}_{-2.47}$	0.0318
KOI-367	27.65 ± 3.56	$25.80^{+1.94}_{-2.08}$	0.1161
KOI-974	10.83 ± 0.12	$4.26^{+0.56}_{-0.41}$	0.0355
KOI-1463	6.042 ± 0.042	$1.64^{+1.36}_{-1.64}$	0.0378

the modeled rotational periods for the KOI systems in Table 3, for which secure spectroscopic parameters are obtained. The derived periods $P_{s,model}$ are listed in Table 4 along with the observed rotational periods P_s . The uncertainty in $P_{s,model}$ comes solely from the uncertainties in M_s and age inferred from spectroscopy, and does not include any systematics in the empirical relation.

The comparison between P_s and $P_{s,model}$ indicates that for most of the systems the rotational periods derived from stellar spots are in reasonably good agreement with the empirical ones, while KOI-261, 974, 1463 show some discrepancies. This suggests that the estimations of either of P_s or spectroscopic parameters may be wrong for those systems. It should also be emphasized, however, that the empirical model by Schlaufman (2010) is rather simplified, and it is difficult to evaluate the systematic errors caused by adopting that empirical relation. For instance, we note that KOI-1463’s host star is so massive that the empirical model may have significant systematics because of the lack of the sampled stars in that region (see Figure 2 in Schlaufman 2010).

There is a non-zero probability that the flux variability is caused by a background star, a probability that is higher, the lower the observed variability is. To investigate this, we estimate the flux variability by taking the detrended mean normalized flux, and eliminating the 5% highest and the 5% lowest values. This step helps to remove the effect of outliers or artifacts that might still remain after the detrending process. The flux variability is then defined as the range of values of the flux. In Table 4, we show the values of the variability for each system. As one can see, KOI-974 and KOI-1463 show a very low level of variability, with a higher false positive probability, whereas KOI-261 is the most active star, which shows that the period of rotation has been calculated more robustly.

Since KOI-261 is apparently the most important system in our sample that most likely to have a spin-orbit misalignment, we pay a special attention to this system. If we adopt the modeled rotational period for KOI-261 as shown in Table 4, we obtain $V_{eq} = 2.27 \pm 0.10$ km s^{-1} , which agrees with its projected rotational velocity of $V \sin I_s = 0.62^{+1.09}_{-0.62}$ km s^{-1} within 2σ . However, as we have shown in Figure 2, the periodogram clearly shows the single strongest peak around 15.5 days. The absence of a peak around 31 days implies that the rotational period is securely derived and does not reflect half the period. We also show in Figure 10 that there exist two

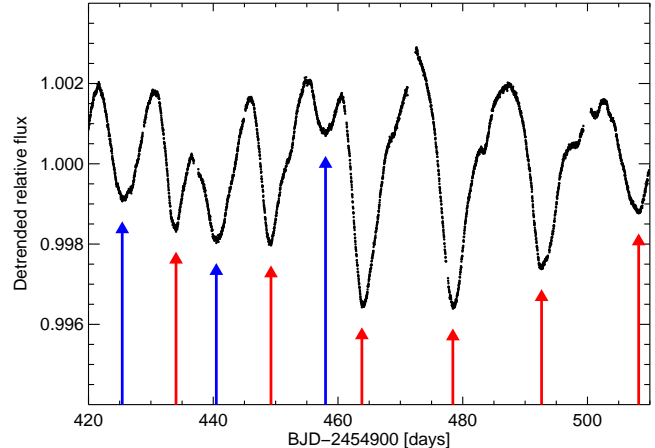


FIG. 10.— The black dots represent the corrected flux series of KOI-261 on a segment of 90 days. In this segment, the star has a peak-to-peak variability of up to 0.6%. The blue and red arrows point to the flux minima generated by two different active regions. The active region represented by blue arrows seems to disappear after three rotation periods, whereas the one represented by red arrows seems to reach its maximum size in the middle of the observations. In both cases, the flux minima recur with a periodicity of 15 days, confirming the value obtained with the Lomb-Scargle periodogram.

active regions on the stellar surface manifested in KOI-261’s lightcurve. The reason for the disagreement between the observed and modeled rotational periods for KOI-261 is unknown, but it is general believed that such active stars as KOI-261 rotate faster. Future confirmation and characterizations of this system is particularly intriguing.

5.3. Impact of Differential Rotation

So far, we have discussed the stellar inclinations I_s assuming no differential rotation of the planet hosting star. In reality, however, stars may have differential rotations, which are supposed to be related to the origin of starspots, and the rotational velocity at the equator may be different from that estimated at the location of the star spot. Here, we discuss the impact of stellar differential rotations on our estimate of I_s .

Following Reiners & Schmitt (2003), we model the angular velocity Ω as a function of the latitude l on the stellar surface as

$$\Omega(l) = \Omega_{eq}(1 - \alpha \sin^2 l), \quad (8)$$

where Ω_{eq} is the angular velocity of the star at the equator. The degree of differential rotation α is about 0.2 for the case of the Sun. In the presence of a differential rotation, it is more explicit to rewrite Equation (1) as

$$\sin I_s = \frac{(V \sin I_s)_{spec}}{R_s \Omega_{eq}(1 - \alpha \sin^2 l)}. \quad (9)$$

Since we do not have information on l where the stellar spot that we observed is located, the uncertainty for l results in a systematic error for $\sin I_s$. A fortunate situation is, however, the spectroscopically measured $V \sin I_s$ in the numerator of Equation (9) is likely estimated to be smaller in the presence of differential rotations ($\alpha > 0$). This is because the solar-type differential rotation leads

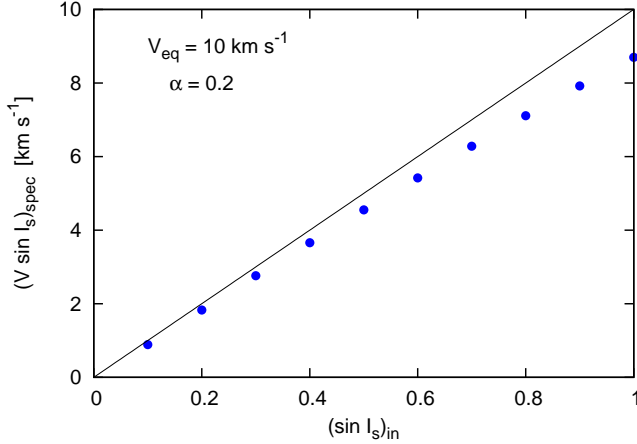


FIG. 11.— The simulated result for the line profile fitting in the presence of differential rotation. We plot the best-fit values for $(V \sin I_s)_{\text{spec}}$ obtained by fitting the line profiles of differential rotation with the rotational kernel for a “rigid rotation”, for various input stellar inclinations $(\sin I_s)_{\text{in}}$. In this plot, we employ $V_{\text{eq}} = 10 \text{ km s}^{-1}$ and $\alpha = 0.2$, and the black line represents the expected $V \sin I_s$ for rigid rotation. The best-fit results for $(V \sin I_s)_{\text{spec}}$ are deviated from the cases for rigid rotation by $\sim 10\%$.

to a “sharper” spectral line profile (Reiners & Schmitt 2003), which results in a smaller value for $V \sin I_s$ when fitted by the rotational broadening kernel for “rigid rotation”. Since the denominator of Equation (9) also becomes smaller in the presence of differential rotation, the impact of differential rotation tends to be more or less compensated.

In order to quantitatively evaluate Equation (9), we perform the following simple numerical simulation. First, we generate the mock line profile by convolving a single Gaussian function with a rotational broadening kernel (including macroturbulence) for a differentially rotating star. The input parameters to create one line profile are the rotational velocity at the equator $V_{\text{eq}} \equiv R_s \Omega_{\text{eq}}$, differential rotation parameter α , and input stellar inclination $(\sin I_s)_{\text{in}}$ ⁷. Then, we fit the resultant line profile with a convolution function between a Gaussian and a rotational broadening kernel for a rigid body, and estimate the best-fit value for $(V \sin I_s)_{\text{spec}}$.

As a result, in the case of $\alpha = 0.2$, the best-fit values for $(V \sin I_s)_{\text{spec}}$ are smaller than the input values of $V_{\text{eq}} \cdot (\sin I_s)_{\text{in}}$ by $\sim 10\%$, for various cases of $(\sin I_s)_{\text{in}}$ (see Figure 11). This result implies that changing $\sin l$ from 0 to 1 in Equation (9) leads to the systematic errors in the output $\sin I_s$ of $\sim \pm 10\%$. We check it for various values of the input parameters V_{eq} , α , and $(\sin I_s)_{\text{in}}$ and find that the relative systematic error in estimating $\sin I_s$ from Equation (9) is approximately 0.5α .

In the case of the Sun, however, the latitudes at which we observe the spots are confined to the relatively narrow bands of $5^\circ \lesssim |l| \lesssim 40^\circ$. The active latitude is known to move toward the solar equator with a cycle of ~ 11 years, making the well-known “butterfly diagram” (e.g., Ruždjak et al. 2005).

In order to correct for the impact of differential rotation, we here adopt the following empirical model for α

⁷ The other parameters such as the original Gaussian width and macroturbulence dispersion are fixed in the simulation.

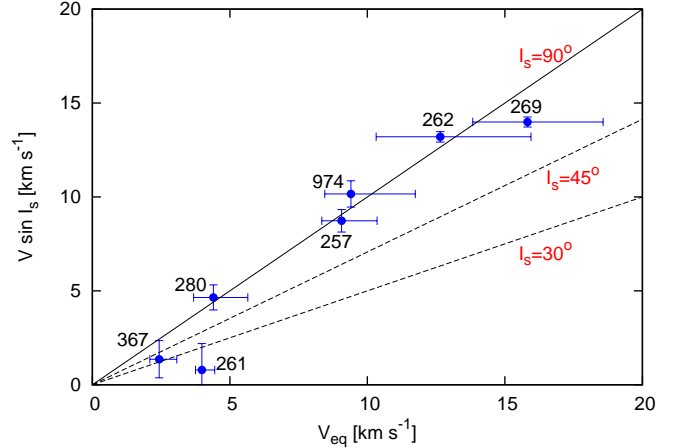


FIG. 12.— Same as Figure 5, after corrected for the impact of differential rotations.

reported by Collier Cameron (2007):

$$\alpha \Omega_{\text{eq}} = 0.053 (T_{\text{eff}}/5130)^{8.6}. \quad (10)$$

This expression, which is based on observations of Doppler imaging or Fourier analyses of the rotational broadening kernel, claims that differential rotations are stronger for hotter stars such as our targets (Collier Cameron 2007; Dunstone et al. 2008). We perform the same simulation using the mock line profile in the presence of differential rotation for each of the seven systems, and then correct for the impact of differential rotation. We evaluate the systematic errors in V_{eq} assuming that the spots are located at $|l| = 20^\circ \pm 20^\circ$, imitating the case of the Sun.

Figure 12 plots thus corrected $V_{\text{eq}} - V \sin I_s$ diagram. In contrast to Figure 5, KOI-257, 269, 367, and 974 are consistent with $I_s = 90^\circ$ with $\sim 1\sigma$, while KOI-261 still seems to have a spin-orbit misalignment. This implies that differential rotations can partially or totally explain the moderate and apparent spin-orbit misalignments for KOI-257, 269, 367, and 974, although we do not conclude so in the present paper because of the rather rough assumptions we adopted for the correction of differential rotation. We note that if this is the case, it is equally interesting in the sense that the present method can reveal the signature of differential rotations of distant transiting planetary systems.

5.4. Comparison with the RM Measurement for Kepler-8

Finally, we briefly discuss the application of the present technique to the confirmed Kepler systems. Specifically, systems where the RM effect has been measured are particularly interesting since we can directly compare between the sky-projected and line-of-sight spin-orbit angles. Among the confirmed Kepler systems with the RM measurements, Kepler-8 shows a periodic flux variation, and we obtain the rotational period of $P_s = 7.5 \pm 0.3$ days. This period, along with the stellar radius of $R_s = 1.486^{+0.067}_{-0.062} R_\odot$ (Jenkins et al. 2010a), results in $V_{\text{eq}} = 10.0 \pm 0.6 \text{ km s}^{-1}$, which is in good agreement with the projected rotational velocity $V \sin I_s = 10.5 \pm 0.7 \text{ km s}^{-1}$ (Jenkins et al. 2010a). Although $I_s \approx 90^\circ$ is

only a requirement for a spin-orbit alignment, this result does not support the RM measurement by Jenkins et al. (2010a) ($\lambda = -26.4^\circ \pm 10.1^\circ$). See also Albrecht (2012), who suspected the uncertainty of λ for Kepler-8 to be underestimated.

6. SUMMARY AND FUTURE PROSPECTS

We have investigated the stellar inclinations for KOI planetary system candidates on the basis of the detailed analyses of photometric variation due to stellar spots and spectroscopic measurements of $V \sin I_s$. We have found that at least one system, KOI-261, exhibits a strong signature of a possible spin-orbit misalignment along the line-of-sight. The planetary candidate KOI-261.01 is a Neptune-sized one ($R_p \approx 3R_\oplus$), with a moderate orbital distance ($a_p \approx 0.13$ AU). If this system is confirmed and eventually turns out to be misaligned, KOI-261.01 will become the smallest planet ever reported to have a spin-orbit misalignment, which makes it an important sample to test and discuss planetary migrations in an extended parameter space. KOI-1463 also shows a small stellar inclination, though the size of the transiting companion may correspond to that of an M star and the periodic signal may come from the companion. The results for the other systems are ambiguous but they may be interpreted as either mildly misaligned or differentially rotating.

One of the next tasks is to increase the number of samples and further discuss the correlations between I_s and other system parameters, for each of the Earth-sized planet population and giant planet population. This will require to choose fainter stars, unless new updates of the catalog bring many candidates around variable hot stars. Even with the currently available dataset, it is relatively easy to plan a more efficient observing run, giving higher priority to stars with a higher variability and ruling out those ones with no variability or with signals that are too coherent to be caused by spots.

It is also important to refine the measurements of I_s . We are potentially able to do so if we combine the spectroscopic measurement with photometric data. For instance, the ratio of the planet semi-major axis to stellar radius is available via transit photometry, but we did not use it in estimating the stellar radius R_s . This is simply because a/R_s generally depends on the orbital eccentric-

ity e , and e cannot be determined by the transit alone unless the secondary eclipse is seen in the lightcurve. If radial velocities for the systems presented in this paper are followed-up by some future observations and their orbital eccentricities are measured, we are able to constrain R_s more precisely and the estimates for $\sin I_s$ would be significantly improved.

Finally, we stress that all the systems that we analyzed are still candidates for having planetary companions, and therefore we must be careful in discussing the evolution history of planetary systems with the present technique. However, we can safely say that possible misaligned systems suggested by our analysis would become very interesting targets for future RM measurements.

This paper is based on data collected at Subaru Telescope, which is operated by the National Astronomical Observatory of Japan. We are very grateful to Simon Albrecht, for helpful comments on this manuscript. We acknowledge the support for our Subaru HDS observations by Akito Tajitsu, a support scientist for the Subaru HDS. T.H. would like to express special thanks to Akihiko Fukui for a fruitful discussion on this subject. The data analysis was in part carried out on common use data analysis computer system at the Astronomy Data Center, ADC, of the National Astronomical Observatory of Japan. T.H. is supported by Japan Society for Promotion of Science (JSPS) Fellowship for Research (DC1: 22-5935). J.N.W. acknowledges support from the NASA Origins program (NNX11AG85G). N.N. acknowledges a support by NINS Program for Cross-Disciplinary Study. Y.S. gratefully acknowledges support from the Global Collaborative Research Fund “A World-wide Investigation of Other Worlds” grant and the Global Scholars Program of Princeton University, the Grant-in-Aid No. 20340041 by JSPS, and JSPS Core-to-Core Program “International Research Network for Dark Energy”. We wish to acknowledge the very significant cultural role and reverence that the summit of Mauna Kea has always had within the indigenous people in Hawai’i. We would like to express special thanks the anonymous referee for the helpful comments and suggestions on this manuscript.

REFERENCES

- Albrecht, S. 2012, in IAU Symposium, Vol. 282, IAU Symposium, 379–384
- Albrecht, S., Reffert, S., Snellen, I., Quirrenbach, A., & Mitchell, D. S. 2007, *A&A*, 474, 565
- Barnes, J. W. 2009, *ApJ*, 705, 683
- Basri, G., et al. 2011, *AJ*, 141, 20
- Batalha, N. M., et al. 2012, *ArXiv e-prints*
- Borucki, W. J., et al. 2010, *Science*, 327, 977
- , 2011, *ApJ*, 736, 19
- Brown, T. M., Latham, D. W., Everett, M. E., & Esquerdo, G. A. 2011, *AJ*, 142, 112
- Chambers, J. E. 2009, *Annual Review of Earth and Planetary Sciences*, 37, 321
- Chatterjee, S., Ford, E. B., Matsumura, S., & Rasio, F. A. 2008, *ApJ*, 686, 580
- Collier Cameron, A. 2007, *Astronomische Nachrichten*, 328, 1030
- Collier Cameron, A., et al. 2010, *MNRAS*, 407, 507
- Désert, J.-M., et al. 2011, *ApJS*, 197, 14
- Dunstone, N. J., Hussain, G. A. J., Collier Cameron, A., Marsden, S. C., Jardine, M., Barnes, J. R., Ramirez Velez, J. C., & Donati, J.-F. 2008, *MNRAS*, 387, 1525
- Fabrycky, D., & Tremaine, S. 2007, *ApJ*, 669, 1298
- Fabrycky, D. C., & Winn, J. N. 2009, *ApJ*, 696, 1230
- Fuhrmann, K. 1998, *A&A*, 338, 161
- Gray, D. F. 2005, *The Observation and Analysis of Stellar Photospheres*, ed. Gray, D. F.
- Hébrard, G., et al. 2008, *A&A*, 488, 763
- , 2011, *A&A*, 533, A130
- Hirano, T., Narita, N., Shporer, A., Sato, B., Aoki, W., & Tamura, M. 2011a, *PASJ*, 63, 531
- Hirano, T., Suto, Y., Winn, J. N., Taruya, A., Narita, N., Albrecht, S., & Sato, B. 2011b, *ApJ*, 742, 69
- Jenkins, J. M., et al. 2010a, *ApJ*, 724, 1108
- , 2010b, *ApJ*, 713, L120
- , 2010c, *ApJ*, 713, L87
- Lanza, A. F., et al. 2009, *A&A*, 493, 193
- Lin, D. N. C., Bodenheimer, P., & Richardson, D. C. 1996, *Nature*, 380, 606
- Lubow, S. H., & Ida, S. 2010, *Planet Migration*, ed. Seager, S., 347–371
- Mayor, M., et al. 2011, *ArXiv e-prints*
- Nagasawa, M., & Ida, S. 2011, *ApJ*, 742, 72

- Nagasawa, M., Ida, S., & Bessho, T. 2008, *ApJ*, 678, 498
Narita, N., Sato, B., Hirano, T., & Tamura, M. 2009, *PASJ*, 61, L35
Narita, N., et al. 2007, *PASJ*, 59, 763
Nutzman, P. A., Fabrycky, D. C., & Fortney, J. J. 2011, *ApJ*, 740, L10
Ohta, Y., Taruya, A., & Suto, Y. 2005, *ApJ*, 622, 1118
Radick, R. R., Mihalas, D., Hartmann, L., Worden, S. P., Africano, J. L., Klimke, A., & Tyson, E. T. 1982, *PASP*, 94, 934
Reiners, A., & Schmitt, J. H. M. M. 2003, *A&A*, 398, 647
Ruždjak, D., Brajša, R., Sudar, D., & Wöhl, H. 2005, *Sol. Phys.*, 229, 35
Sanchis-Ojeda, R., & Winn, J. N. 2011, *ApJ*, 743, 61
Sanchis-Ojeda, R., Winn, J. N., Holman, M. J., Carter, J. A., Osip, D. J., & Fuentes, C. I. 2011, *ApJ*, 733, 127
Schlaufman, K. C. 2010, *ApJ*, 719, 602
Smith, J. C., et al. 2012, *ArXiv e-prints*
Stumpe, M. C., et al. 2012, *ArXiv e-prints*
Takeda, Y. 1995, *PASJ*, 47, 337
Takeda, Y., Ohkubo, M., & Sadakane, K. 2002, *PASJ*, 54, 451
Takeda, Y., Ohkubo, M., Sato, B., Kambe, E., & Sadakane, K. 2005, *PASJ*, 57, 27
Triaud, A. H. M. J. 2011, *A&A*, 534, L6+
Triaud, A. H. M. J., et al. 2010, *A&A*, 524, A25+
Valenti, J. A., & Fischer, D. A. 2005, *ApJS*, 159, 141
Winn, J. N., Fabrycky, D., Albrecht, S., & Johnson, J. A. 2010a, *ApJ*, 718, L145
Winn, J. N., Johnson, J. A., Albrecht, S., Howard, A. W., Marcy, G. W., Crossfield, I. J., & Holman, M. J. 2009, *ApJ*, 703, L99
Winn, J. N., et al. 2005, *ApJ*, 631, 1215
—. 2010b, *ApJ*, 723, L223
Wu, Y., & Murray, N. 2003, *ApJ*, 589, 605
Yi, S., Demarque, P., Kim, Y.-C., Lee, Y.-W., Ree, C. H., Lejeune, T., & Barnes, S. 2001, *ApJS*, 136, 417